



PAPER

OPEN ACCESS

RECEIVED
31 October 2025REVISED
2 February 2026ACCEPTED FOR PUBLICATION
16 March 2026PUBLISHED
7 April 2026

Original content from this work may be used under the terms of the [Creative Commons Attribution 4.0 licence](#).

Any further distribution of this work must maintain attribution to the author(s) and the title of the work, journal citation and DOI.



An artifact-robust framework for measuring tES effects during stimulation

Nima Noury^{1,2,3,4,*} , Fabio Damiani^{1,2,3} and Markus Siegel^{1,2,3,4,5,*} ¹ Department of Neural Dynamics and Magnetoencephalography, Hertie Institute for Clinical Brain Research, University of Tübingen, Tübingen, Germany² Centre for Integrative Neuroscience, University of Tübingen, Tübingen, Germany³ MEG Center, University of Tübingen, Tübingen, Germany⁴ Center for Bionic Intelligence Tübingen Stuttgart (BITS), Tübingen, Germany⁵ German Center for Mental Health (DZPG), Tübingen, Germany

* Authors to whom any correspondence should be addressed.

E-mail: nima.noury@uni-tuebingen.de and markus.siegel@uni-tuebingen.de

Keywords: tACS, MEG, artifacts, visual flicker, interaction, brain-state dependency

Abstract

Objective. Transcranial electric stimulation (tES) is a promising technique to non-invasively modulate human brain activity. However, stimulation artifacts in EEG and MEG recordings severely hinder the study of its online effects. **Approach.** Here, we introduce a new approach to account for these artifacts. The approach rests on two key ideas. First, we focus on interactions of tES with intrinsic brain activity, which are absent for tES artifacts. Second, rather than removing artifacts, we compare composite signals that share similar artifacts but potentially differ in the interaction of tES with intrinsic brain activity. We follow a simple logic: if tES does not interact with intrinsic brain activity, then neural activity during simultaneous sensory stimulation and tES should equal the linear superposition of the neural effects of each applied alone. Any deviation from this prediction provides evidence for a neural interaction. **Main results.** We tested this approach in a proof-of-principle MEG study, applying 10 Hz transcranial alternating current stimulation (tACS) during rest and during a 10 Hz visual flicker. We compared neural activity during simultaneous stimulation with that predicted by the linear superposition of flicker and tACS alone and found a phase-dependent interaction between tACS and flicker-evoked brain activity. **Significance.** Our work establishes a novel approach to investigate online effects of tES and suggests a state-dependent interaction of tACS with human brain activity.

1. Introduction

Transcranial electric stimulation (tES) is a non-invasive brain stimulation technique, which allows control over stimulation strength, frequency and—to some extent—stimulation site [1–7]. These features render tES an attractive technique for manipulating specific brain rhythms [8–10]. The potential of electrical stimulation to modulate neuronal oscillations has been demonstrated in animal models [11–14]. However, despite progress [15–18], stimulation artifacts remain a major challenge for investigating modulations of human brain activity during stimulation, and it has been argued that prior findings may have been contaminated by residual artifacts [19–22].

Here, we propose a novel approach to study online effects of tES while accounting for stimulation artifacts. Our approach rests on two key ideas. First, behavioral and offline effects of tES depend on the state of ongoing brain activity, indicating that online effects may arise through interactions of tES and intrinsic brain activity [9, 11, 23–33]. Such interactions are, by definition, absent for mere tES artifacts. Thus, our approach aims to identify interactions of tES with intrinsic brain activity. We therefore test for interactions by controlling intrinsic activity with sensory stimulation and asking whether neural activity during simultaneous sensory stimulation and tES matches the linear superposition of the effects of each applied alone. Any deviation from linear

superposition indicates an interaction between tES and intrinsic activity. Second, because tES artifacts are non-linear and several orders of magnitude larger than intrinsic signals [19–22, 34] we avoid attempting to subtract artifacts from recorded signals. Instead, we construct and compare composite signals that are matched in artifact level but potentially differ in whether they contain interactions between tES and intrinsic brain activity.

We implemented this approach in a proof-of-principle magnetoencephalography (MEG) study. We induced a well-controlled 10 Hz brain rhythm using visual flicker (steady-state response) and simultaneously applied 10 Hz transcranial alternating current stimulation (tACS) at different phase relations to the flicker. This allowed us to test whether our approach reveals neural interactions between tACS and intrinsic brain activity during stimulation. We observed clear deviations from the linear prediction, indicating phase-dependent interactions between tACS and intrinsic brain activity.

2. Materials and methods

2.1. Participants and experimental protocol

Sixteen healthy subjects participated in this study. All subjects provided written informed consent and were financially compensated. The study was carried out in accordance with the Declaration of Helsinki and was approved by the Ethics Committee at the Medical Faculty of the Eberhard Karls University and at the University Hospital of Tübingen. None of the subjects reported a history of psychiatric/neurological disorders or any other contraindications of tACS.

Each subject participated in six blocks of 280 trials (i.e. $6 \times 280 = 1680$ trials in total). Seven distinct conditions were applied (figure 2). These conditions were arranged in randomized seven-trial sequences such that each condition was applied once before a new seven-trial sequence began. This resulted in 40 trials per condition per block (i.e. $7 \times 40 = 280$ trials per block in total). Of the seven conditions, one condition only contained a 10 Hz visual flicker stimulus (V), and two contained only 10 Hz tACS, one with an initial phase of 0 (T_0) and the other one with an initial phase of π (T_π). The remaining 4 conditions contained simultaneous 10 Hz visual flicker and 10 Hz tACS, and each had a phase difference of either 0, π , $\frac{\pi}{2}$, or $\frac{3\pi}{2}$ between the two (VT_0 , VT_π , $VT_{\pi/2}$, $VT_{3\pi/2}$, respectively). VT_0 and VT_π were constructed by simultaneous application of V and T_0 or T_π conditions, respectively. To construct $VT_{\pi/2}$ and $VT_{3\pi/2}$ conditions, we also combined V and T_0 or T_π conditions but started V signals 25 ms (i.e. $\frac{\pi}{2}$ radians at 10 Hz) earlier than for the original V condition (figure 2). We used signals after tACS offset of T_0 and T_π conditions

as rest signals (R , details explained below, see also the discussion section).

Each trial was 1.2 s long, and was followed by an inter-trial interval (ITI) with a random length that was uniformly distributed from 1 to 1.4 s. During all conditions, subjects were required to simply focus on a white fixation point. After every second ITI, the fixation dot changed from white to blue for one second. Subjects were asked to restrict their eye blinking to this interval. This helped us to minimize blinking artifacts.

2.2. Visual flicker stimulus

Visual stimuli were presented on a back-projection screen using a projector with 60 Hz refresh rate. The visual flicker stimulus was constructed of 10 flashes. Each flash was 1 frame long and successive flashes were 6 frames apart from each other, which yields a visual flicker at 10 Hz. On each flash, a white narrow horizontal rectangle on a black background at full contrast was shown. We chose this shape to optimize the simultaneity of the retinal input because the projector rendered each frame in horizontal lines from top to bottom. Specifically, we set the height of the rectangle such that there was a 2 ms delay between the onset of the top and bottom edges of the white rectangle (i.e. 7.2° at 10 Hz). A fixation dot was shown during the entire experiment. During flashes, we presented the fixation dot on a small black circle. The fixation dot was white, except for eye-blinking intervals, during which it turned blue. Stimulus presentation was designed and controlled via custom scripts using Psychtoolbox-3 [35]. After each experiment, we checked the timing of the presented frames as reported by Psychtoolbox and did not observe any frame drops or refresh rate distortions. Moreover, we used a photodiode to further verify the timing of the visual flicker stimulus (explained below) and did not observe any distortion in the 10 Hz visual flicker.

2.3. Transcranial current stimulation

The stimulation current was applied with an IZ2H stimulator (Tucker Davis Technologies Inc.) driven by an LZ48-400 battery pack. The 10 Hz tACS signal was generated by an RZ5D BioAmp Processor and was controlled via processing chains that were created using the RPvdsEx Visual Design software. These processing chains were activated using custom-written Matlab scripts, which made use of the ActiveX software framework to send commands to the signal generator. Stimulation was applied via two 35 cm² rubber electrodes (neuroConn GmbH), which were attached using Ten20 conductive paste (Weaver and Company).

The electrodes were positioned such that the top edge of the first electrode lay over the midline parietal location (PZ) and the top edge of the second electrode lay over the inion (IZ). Cables ran over the right

shoulder. This montage was chosen to ensure that the spatial focus of the induced electric field would be close to primary visual cortex. This was validated using SimNIBS [36] (figure 2).

In each trial, the stimulation current was linearly ramped up from zero to the maximum intensity over a period of 250 ms to minimize the possibility of unpleasant tactile sensations. At the end of each trial, stimulation stopped at zero amplitude after precisely 12 cycles.

The maximum value of the tACS current was determined for each subject as follows: Electrodes were attached to the chosen scalp locations using conductive gel. Starting at 0.1 mA (peak amplitude), tACS was applied for approximately ten cycles. The intensity was then increased by 0.05 mA without the subject's knowledge. This incremental increase continued until the subject reported either phosphene perception or any tactile sensation at the electrode locations. At this point the current was decreased by 0.05 mA and the magnitude was recorded for future reference. The electrodes were then secured with gauze and tape, after which the procedure was repeated in a darkened room, to ensure that any phosphene perception would be more pronounced. This time, tACS application began at the previously recorded threshold, and was incrementally increased without the subjects' knowledge after ten cycles, as before. As soon as phosphene perception was reported, the intensity was decreased and the current was applied again for ten cycles. Depending on feedback from the subject, the intensity would either be increased or decreased. This gradual adjustment continued until the subject reported that no phosphenes were visible. The subject-specific tACS intensity used during the experiment was ultimately chosen to be 0.05 mA lower than the maximum current at which no phosphenes were perceived. The procedure resulted in subject-specific intensities ranging from 0.25 mA to 0.9 mA (stimulation intensity of all subjects in mA: .30, .40, .40, .45, .90, .30, .30, .50, .30, .45, .30, .30, .60, .30, .40, .25. Note that peak-to-peak values would be two times bigger).

We corrected the difference in the internal clock of the tACS stimulator and the clock of the visual flicker computer as follows. We used a photodiode on the monitor to record the exact timing of the visual flicker and recorded its output with the A/D converter of the MEG recording console. Moreover, using the same A/D converter we recorded the tACS stimulation current by measuring the voltage drop across a 200 Ω resistor positioned in series to the head. Next, we carefully adjusted the frequency of the tACS signal until the frequency of the 2 measured signals matched. In addition, due to the response time of the projector, we found a delay of approximately 30 ms between the execution of the Matlab command for flicker presentation and the appearance of the flicker

on the projector screen. This was corrected by introducing an extra time delay before tACS onset at the beginning of each trial, which again was determined by careful inspection of the photodiode and tACS voltage traces.

2.4. Data acquisition and preprocessing

We recorded 272-channel MEG (Omega 2000, CTF Systems) throughout the experiment at 2343.8 Hz sampling rate. All signals were in the dynamic range of the recording system and no clipping was observed. Due to the interference between stimulation currents and electrical currents of the head-positioning circuits of the MEG system, we could not monitor head movement continuously during the experiment. We recorded ECG signals using bipolar channels of the MEG system. The ECG was recorded through 2 electrodes placed below the right clavicle and below the left pectoral muscle.

We manually inspected all data and removed all parts of the data with physiological or technical artifact. We defined the start of trials as the start of the flicker stimulus in the *V* condition, and as the start of the tACS stimulus in all other conditions. Then, we segmented the data into 2.4 s intervals, starting 200 ms before trial onset, and linearly detrended each interval (removing a linear fit from each interval, Matlab `detrend`-function).

We generated time-shifted copies of trials from the *V* condition, which in the following we term $V_{\frac{\pi}{2}}$. This was done by shifting these trials 25 ms (i.e. $\frac{\pi}{2}$ radian in 10 Hz) backward in time. These copies were later used for constructing the composite signals.

Because of the difference between the clocks of the MEG recording console and of the tACS stimulator, the tACS frequency appears slightly different from 10 Hz in MEG recordings. Due to the strong stimulation artifacts, such subtle clock differences can lead to measurable distortions in the recorded signals. In fact, tACS artifacts at 1 mA peak-to-peak can be up to 10 000 times larger than neural signals [20, 21]. Consequently, the difference between two sine waves at 10.0007 Hz and 10 Hz evaluated 850 ms after onset (i.e. the duration of the segments used for subsequent detrending) can be up to 37 times larger than the underlying brain activity ($10000 * [\sin(2\pi * 10 * 0.85) - \sin(2\pi * 10.0007 * 0.85)] = 37$). To minimize such distortions, we corrected for the clock differences between the stimulation and recording systems. We manually selected several intervals of MEG data with stable tACS artifacts from the first recorded subject and estimated their stimulation frequency by fitting a sine wave to each interval (Matlab `nlinfit`-function). We then took the median of the estimated stimulation frequencies (10.000 711 273 294 087 Hz). Next, we redefined the time of all MEG data (Matlab `interp1`-function) to place the recorded stimulation frequency

at exactly 10 Hz. Moreover, we resampled the data to 2360 Hz to ensure that the sampling rate was divisible by the stimulation frequency. This helped, at later stages, to obtain FFT estimates exactly at 10 Hz, i.e. at the frequency of interest.

To prevent temporal leakage of stimulation artifacts to the post-stimulation interval, we did not apply any filtering to the data. However, to improve estimates of spectral content at 10 Hz, it was necessary to remove slow drifts of data by detrending. Detrending decreases the spectral leakage from lower frequencies to 10 Hz. To this end, we first cut two 850 ms long segments (i.e. 8.5 cycles at 10 Hz) out of each 2.4 s interval, one segment from 350 ms after start of the trial to the end of stimulation, and the other segment starting 150 ms after the end of the stimulation. We refer to the former as during-stimulation segments (y_{during}), and to latter as post-stimulation segments (y_{post}). We chose this exact length to improve the performance of linear de-trending for segments with strong tACS artifacts. This is because, the artifact phase at MEG channels with highest tACS artifacts is either close to 0° or 180° [21]. Because a sine wave with a phase near 0° or 180° is temporally symmetric over a duration of $n + \frac{1}{2}$ cycles, linear detrending does not distort it or introduce artifacts. It is worth noting that the initial tACS ramp-up lasted 250 ms. Therefore, the during-stimulation segments and the subsequent detrending were not affected by it. Next, we linearly detrended each during-stimulation and post-stimulation segment and discarded the first 50 ms of each segment.

In sum, preprocessing resulted in two segments of data for each trial. Both segments were exactly 800 ms long (i.e. 8 cycles at 10 Hz). The during-stimulation segments extended from 400 ms after start of the stimulation to the end of the stimulation. The post-trial segments started 200 ms after stimulation offset. Moreover, the data were resampled in a way that the tACS frequency was recorded at exactly 10 Hz, and that applying FFT to them would provide a spectral estimate at exactly 10 Hz.

For each block (280 trials, i.e. 40 trials per condition), we concatenated all during- and post-stimulation pieces, calculated the beamforming spatial filter, and projected the data to source-space. We used adaptive linear spatial filtering (beamforming) [37] with zero regularization factor (λ) [19]. To get one estimate at each source location, we calculated three orthogonal filters (one for each spatial dimension), projected the data through them, and linearly combined them in the direction of the maximum variance.

2.5. Source locations and physical forward model

We performed the beamforming analysis on a regular three-dimensional grid that covered an SPM's template brain with 1 cm spacing in MNI space (4805 source locations, `spm8/templates/T1.nii`). We used

fieldtrip's template T1-weighted structural MRI for all subjects (`template/headmodel/standard_mri.mat`) and nonlinearly transformed source locations into head space. The MEG sensors were aligned to the head geometry on the basis of three fiducial points (nasion, left ear, right ear) that were registered before and after the MEG acquisition by three head localization coils. To derive the physical relation between sources and sensors (leadfield), we employed a single-shell head model [38].

2.6. Spectral analysis

We applied FFT to each 800 ms data segment at the source level and took the spectral content at 10 Hz for further analysis.

For each subject and voxel, we computed the complex phase-locking value (PLV) and the pairwise phase consistency (PPC), the latter providing an unbiased measure of phase locking across trials [39]:

$$\text{PLV}_{\text{complex}} = \frac{1}{N} \sum_{j=1}^N \exp^{i\theta_j} \quad (1)$$

$$\text{PPC} = \frac{2}{N(N-1)} \sum_{j=1}^{N-1} \sum_{k=(j+1)}^N \cos(\theta_j - \theta_k) \quad (2)$$

where θ is the phase of each 800 ms segment at 10 Hz and N denotes the number of trials. As a measure of power, we calculated the decimal logarithm of the absolute value of FFT results, and took the average across trials, for each voxel and subject.

2.7. Contrasting conditions

We employed cluster permutation statistics to contrast source-level parameters between various conditions (figure 3). For each subject, voxel, and condition, we first obtained the mean 10 Hz power across trials (or PPC). Then, at each voxel, we concatenated values of the two compared conditions of all subjects, which resulted in a vector with 32 samples. We normalized this vector by histogram matching (Gaussian), and obtained a zero-mean normal vector, but kept its standard deviation. Next, at each voxel, we took the difference between the two conditions and calculated its t -statistic across subjects. Finally, we employed a cluster sign-flip permutation test on these values. Specifically, we defined spatial clusters of voxels whose t -values exceeded a threshold of 2.581 (or were below -2.581 when testing for negative clusters), using a minimal-neighborhood criterion to determine spatial contiguity. Then, we averaged t -values of all voxels of each cluster.

Next, we estimated the null-distribution by randomly flipping the sign of the normalized power (or PPC) differences of each subject (same flip for all voxels of each subject), calculating the t -statistic across subjects, defining clusters, and calculating

mean t -value of each cluster. Importantly, we retained only the cluster with the largest mean t -value across all clusters to control the familywise error rate [40]. To this end, we constructed the null-distribution by repeating the sign flipping procedure 1000 times and keeping the maximum cluster-level value from each permutation. Finally, we assigned a p -value to each cluster of the original data by comparing its averaged t -value against this null-distribution.

From the contrast between visual flicker only (V) and rest (R) conditions (figure 3(d)), we defined a region of interest (ROI), in which we subsequently tested for the interaction of tACS and visual flicker, i.e. for cluster permutation tests used to compare composite signals. This ROI was created by combining the power and phase clusters that showed significant differences between the V and R conditions.

2.8. TACS offset artifact

To avoid contamination of post-stimulation segments by residual tACS offset artifacts, we defined these segments to begin 200 ms after tACS offset. Moreover, we did not apply filtering to our data, because any filtering would spread artifacts across time. We performed several tests to ensure that post-stimulation segments did not contain any tACS offset artifacts. As the first test, we argued that tACS conditions that have anti-phase tACS signals, should also show anti-phase tACS offset artifacts. Thus, if post-stimulation segments were contaminated by offset-artifacts, their PLV_{complex} vectors should point to opposite phases. We tested this using a cluster permutation test, in which we took the difference of PLV_{complex} vectors of two corresponding tACS conditions and compared the length of the resulting vector against the null-distribution. We constructed the null-distribution by randomly flipping the sign of PLV_{complex} of subjects (similar to *contrasting conditions*, but with a threshold of 1.96 to increase the sensitivity). We did not observe any significant difference (T_0 against T_π , $p > 0.65$). We performed additional cluster permutation tests to investigate if there was any significant difference between power or PPC of post-stimulation segments of tACS conditions with anti-phase tACS signals. None of these comparisons showed a significant difference (T_0 against T_π , $P_{\text{power}} > 0.3$, $P_{\text{PPC}} > 0.16$). In sum, we concluded that the post-stimulation segments were not contaminated by tACS artifacts. It is worth noting that these results further suggest that the post-stimulation segments of tACS alone conditions did not contain outlasting neural effects of tACS, as such effects would be expected to manifest as phase- or power-specific differences between tACS conditions with opposite phases.

2.9. Composite signals

We added up signals of different conditions to construct composite signals x and \hat{x} (figures 4 and 5).

These composite signals implement the linear superposition logic: if simultaneous stimulation equals the linear prediction, no interaction is present; any deviation indicates a neural effect. We constructed 800 ms long x signals by summing during-stimulation segments of the VT conditions with rest segments (R), which were defined as post-stimulation segments of the T conditions (figure 2). As there were only two rest conditions but four x signals, each rest condition had to be used twice. Therefore, we randomly attributed each rest to one of the x signals, as following:

$$x_0(t) = y_{\text{post}, T_0}(t) + y_{\text{during}, VT_0}(t) \quad (3)$$

$$x_{\frac{\pi}{2}}(t) = y_{\text{post}, T_\pi}(t) + y_{\text{during}, VT_{\frac{\pi}{2}}}(t) \quad (4)$$

$$x_\pi(t) = y_{\text{post}, T_0}(t) + y_{\text{during}, VT_\pi}(t) \quad (5)$$

$$x_{\frac{3\pi}{2}}(t) = y_{\text{post}, T_\pi}(t) + y_{\text{during}, VT_{\frac{3\pi}{2}}}(t). \quad (6)$$

We constructed 800 ms \hat{x} signals by summing up during-stimulation segments of V and T conditions:

$$\hat{x}_0(t) = y_{\text{during}, V}(t) + y_{\text{during}, T_0}(t) \quad (7)$$

$$\hat{x}_{\frac{\pi}{2}}(t) = y_{\text{during}, V_{\frac{\pi}{2}}}(t) + y_{\text{during}, T_0}(t) \quad (8)$$

$$\hat{x}_\pi(t) = y_{\text{during}, V}(t) + y_{\text{during}, T_\pi}(t) \quad (9)$$

$$\hat{x}_{\frac{3\pi}{2}}(t) = y_{\text{during}, V_{\frac{3\pi}{2}}}(t) + y_{\text{during}, T_\pi}(t). \quad (10)$$

As we were interested in the 10 Hz spectral content, instead of first constructing the x and \hat{x} signals in the time domain and then estimating their 10 Hz spectral component, we equivalently first estimated the 10 Hz components of all data segments at the source level and then added up the frequency domain components to estimate the 10 Hz components of x and \hat{x} .

Furthermore, to quantify power and PPC modulations of x_θ and \hat{x}_θ by θ (figure 5), we constructed corresponding $\Delta_{\theta, \theta+\pi}$ and $\widehat{\Delta}_{\theta, \theta+\pi}$ samples, as follows:

$$\Delta_{\text{pow}_{\theta, \theta+\pi}} = \text{pow}(x_\theta) - \text{pow}(x_{\theta+\pi}) \quad (11)$$

$$\widehat{\Delta}_{\text{pow}_{\theta, \theta+\pi}} = \text{pow}(\hat{x}_\theta) - \text{pow}(\hat{x}_{\theta+\pi}) \quad (12)$$

$$\Delta_{\text{ppc}_{\theta, \theta+\pi}} = \text{ppc}(x_\theta) - \text{ppc}(x_{\theta+\pi}) \quad (13)$$

$$\widehat{\Delta}_{\text{ppc}_{\theta, \theta+\pi}} = \text{ppc}(\hat{x}_\theta) - \text{ppc}(\hat{x}_{\theta+\pi}) \quad (14)$$

for $\theta = 0$ and $\frac{\pi}{2}$.

2.10. Null model and analysis pipeline

First, we compared power and PPC of composite signals against each other (e.g. x_0 against \hat{x}_0 , figure 4). To this end, we employed the same cluster permutation tests as for power and PPC of regular conditions (see *contrasting conditions*, we used a threshold of 1.96 for tests on composite signals to increase the sensitivity).

In another cluster permutation test (figure 5), we compared $|\Delta_{\theta, \theta+\pi}|$ with its corresponding $|\hat{\Delta}_{\theta, \theta+\pi}|$, for $\theta = 0$ and $\frac{\pi}{2}$, and for power and PPC ($|\cdot|$ refers to absolute value). Given how the composite signals were constructed (equations (3)–(10)), it is clear that x_θ and \hat{x}_θ signals at different values of θ were not statistically independent. For example, all \hat{x}_θ signals used the same trials of $y_{\text{during}, V}$ (or its time shifted versions). These interdependencies complicate the comparison of $|\Delta_{\theta, \theta+\pi}|$ and $|\hat{\Delta}_{\theta, \theta+\pi}|$ by decreasing the degrees of freedom, which in turn affects the $|\Delta_{\theta, \theta+\pi}|$ and $|\hat{\Delta}_{\theta, \theta+\pi}|$ estimates. Importantly, different levels of interdependencies may lead to a spurious difference between $|\Delta_{\theta, \theta+\pi}|$ and $|\hat{\Delta}_{\theta, \theta+\pi}|$. To prevent any false positives due to this issue, we grouped trials into odd and even trials, and constructed new x_θ and \hat{x}_θ signals based either only on odd trials ($x_{\theta, \text{odd}}$ and $\hat{x}_{\theta, \text{odd}}$) or only on even trials ($x_{\theta, \text{even}}$ and $\hat{x}_{\theta, \text{even}}$). Next, we used independent pairs of these new composite signals to generate new delta signals:

$$\Delta \text{pow}_{\theta_{\text{odd}}, \theta+\pi_{\text{even}}} = \text{pow}(x_{\theta, \text{odd}}) - \text{pow}(x_{\theta+\pi, \text{even}}) \quad (15)$$

$$\Delta \widehat{\text{pow}}_{\theta_{\text{odd}}, \theta+\pi_{\text{even}}} = \text{pow}(\hat{x}_{\theta, \text{odd}}) - \text{pow}(\hat{x}_{\theta+\pi, \text{even}}) \quad (16)$$

for $\theta = 0$ and $\frac{\pi}{2}$ (similarly for PPC). For simplicity, we refer to these as $\Delta_{\theta, \text{odd}}$ and $\hat{\Delta}_{\theta, \text{odd}}$. The other option for using independent pairs would be:

$$\Delta \text{pow}_{\theta_{\text{even}}, \theta+\pi_{\text{odd}}} = \text{pow}(x_{\theta, \text{even}}) - \text{pow}(x_{\theta+\pi, \text{odd}}) \quad (17)$$

$$\Delta \widehat{\text{pow}}_{\theta_{\text{even}}, \theta+\pi_{\text{odd}}} = \text{pow}(\hat{x}_{\theta, \text{even}}) - \text{pow}(\hat{x}_{\theta+\pi, \text{odd}}) \quad (18)$$

for $\theta = 0$ and $\frac{\pi}{2}$ (similarly for PPC). For simplicity, we refer to these as $\Delta_{\theta, \text{even}}$ and $\hat{\Delta}_{\theta, \text{even}}$. Pay attention that, in each of these new variables, no trial is used twice. Therefore, it is valid to compare $|\Delta_{\theta, \text{odd}}|$ against $|\hat{\Delta}_{\theta, \text{odd}}|$, and $|\Delta_{\theta, \text{even}}|$ against $|\hat{\Delta}_{\theta, \text{even}}|$. This procedure ensured that any observed differences between composite signals could not arise from statistical dependencies between the constituent trials.

Ideally, one would want to either combine these two tests into one test, or combine their results. Next, we present a method to combine these two tests into one test. We first explain that the presented method leads to asymmetric null-distributions,

which complicates the use of permutation tests. Then, we describe a transformation to solve this issue.

One idea to combine the two tests might be to take the average of $|\Delta_{\theta, \text{odd}}|$ and $|\Delta_{\theta, \text{even}}|$ (i.e. $\frac{|\Delta_{\theta, \text{odd}}| + |\Delta_{\theta, \text{even}}|}{2}$), and compare it against the average of $|\hat{\Delta}_{\theta, \text{odd}}|$ and $|\hat{\Delta}_{\theta, \text{even}}|$ (i.e. $\frac{|\hat{\Delta}_{\theta, \text{odd}}| + |\hat{\Delta}_{\theta, \text{even}}|}{2}$), using a sign-flip permutation test. However, such a test would be biased towards false positives, because some of the trials used in $|\Delta_{\theta, \text{odd}}|$ and $|\hat{\Delta}_{\theta, \text{odd}}|$, are also used in $|\Delta_{\theta, \text{even}}|$ and $|\hat{\Delta}_{\theta, \text{even}}|$ (e.g. looking at equations (7)–(10), (16) and (18)), it is clear that both even and odd trials of $y_{\text{during}, V}(t)$ are used in both $|\hat{\Delta}_{\theta, \text{odd}}|$ and $|\hat{\Delta}_{\theta, \text{even}}|$. Therefore, $|\Delta_{\theta, \text{odd}}|$ and $|\Delta_{\theta, \text{even}}|$, and also $|\hat{\Delta}_{\theta, \text{odd}}|$ and $|\hat{\Delta}_{\theta, \text{even}}|$ are not independent from each other. Importantly, the amount of statistical dependency in the former pair could be different from the latter pair. Therefore, under the null hypothesis, at each voxel and across subjects, $\frac{|\Delta_{\theta, \text{odd}}| + |\Delta_{\theta, \text{even}}|}{2}$ and $\frac{|\hat{\Delta}_{\theta, \text{odd}}| + |\hat{\Delta}_{\theta, \text{even}}|}{2}$ have positively skewed distributions with equal mean but potentially different variances. Hence, under the null hypothesis, at each voxel and across subjects,

$$\frac{|\Delta_{\theta, \text{odd}}| + |\Delta_{\theta, \text{even}}|}{2} - \frac{|\hat{\Delta}_{\theta, \text{odd}}| + |\hat{\Delta}_{\theta, \text{even}}|}{2} \quad (19)$$

could be non-symmetrically distributed around zero. This is problematic, because a sign-flip permutation test assumes a symmetric zero mean null-distribution [41].

We avoided this problem using an intermediate transformation step. For each voxel, we concatenated $|\Delta_{\theta, \text{odd}}|$, $|\hat{\Delta}_{\theta, \text{odd}}|$, $|\Delta_{\theta, \text{even}}|$, and $|\hat{\Delta}_{\theta, \text{even}}|$ values of all subjects (i.e. $N = 4 \times 16 \times 2 = 128$ samples per voxel), and used histogram matching to transform the resulting distribution to a zero-mean normal distribution with unchanged variance. We call these new values $\mathcal{N}\{|\Delta_{\theta, \text{odd}}|\}$, $\mathcal{N}\{|\hat{\Delta}_{\theta, \text{odd}}|\}$, $\mathcal{N}\{|\Delta_{\theta, \text{even}}|\}$, and $\mathcal{N}\{|\hat{\Delta}_{\theta, \text{even}}|\}$. Next, similar to equation (19), for each voxel and subject, we combined these variables by averaging and taking the difference, as

$$\frac{\mathcal{N}\{|\Delta_{\theta, \text{odd}}|\} + \mathcal{N}\{|\Delta_{\theta, \text{even}}|\}}{2} - \frac{\mathcal{N}\{|\hat{\Delta}_{\theta, \text{odd}}|\} + \mathcal{N}\{|\hat{\Delta}_{\theta, \text{even}}|\}}{2} \quad (20)$$

Under the null hypothesis, this new variable has a symmetric zero-mean distribution across subjects (see also *simulation* below). Finally, we performed a sign-flip cluster permutation test on the population-level t -statistic of this variable.

In another cluster permutation test, we repeated the above analysis, comparing $\Delta_{\theta, \text{odd}}$, $\Delta_{\theta, \text{odd}}$, $\Delta_{\theta, \text{even}}$, and $\hat{\Delta}_{\theta, \text{even}}$, i.e. not taking the absolute values.

2.11. Simulation

To ensure that the employed statistical procedure (equation (20)) did not lead to any false positives, we performed a simulation in which we generated a different level of statistical dependency between $|\Delta_{\theta, \text{odd}}|$ and $|\Delta_{\theta, \text{even}}|$, compared to the statistical dependency between $|\hat{\Delta}_{\theta, \text{odd}}|$ and $|\hat{\Delta}_{\theta, \text{even}}|$. More specifically, under the null-hypothesis, we simulated an extreme case, in which we assigned independent random values to $|\Delta_{\theta, \text{odd}}|$ and $|\Delta_{\theta, \text{even}}|$ (i.e. zero dependency), but set values of $|\hat{\Delta}_{\theta, \text{odd}}|$ equal to values of $|\hat{\Delta}_{\theta, \text{even}}|$ (i.e. full dependency).

To this end, for each subject and voxel, we constructed a vector of 16 elements by concatenating power values of all odd and even composite signals of all conditions (i.e. $x_{\theta, \text{odd}}$, $x_{\theta, \text{even}}$, $\hat{x}_{\theta, \text{odd}}$, and $\hat{x}_{\theta, \text{even}}$, for $\theta = 0, \frac{\pi}{2}, \pi, \frac{3\pi}{2}$). Then, for each subject, we calculated the mean of each voxel's vector, and also their covariance matrix across the brain. Next, we drew random samples from a multivariate normal distribution with the empirically measured mean and covariance, and assigned them to $|\Delta_{\theta, \text{odd}}|$, $|\Delta_{\theta, \text{even}}|$, $|\hat{\Delta}_{\theta, \text{odd}}|$. Importantly, we set $|\hat{\Delta}_{\theta, \text{even}}|$ equal to $|\hat{\Delta}_{\theta, \text{odd}}|$ to induce the extreme case of full dependence between them. We applied the same procedure for all subjects, and, finally, applied the same cluster test to these randomly generated dataset as in the main dataset (equation (20)).

We repeated this procedure 1000 times and tested if the resulting p -values were distributed uniformly. Indeed, a two-sample Kolmogorov–Smirnov test did not yield a significant difference between the distribution of p -values and a uniform distribution ($P > 0.1$). Thus, we concluded that the employed statistic was unbiased and did not inflate the false positive rate.

2.12. Spectral profile of the interaction effect

To examine the spectral profile of the observed interaction between tACS and visual flicker, we computed the same test statistic that revealed the significant 10 Hz cluster (equation (20)) at all frequencies up to 100 Hz with a spectral resolution of 1.25 Hz. For each frequency, we averaged the resulting statistic across all voxels within the 10 Hz cluster (figure 6(a)) to obtain a spectrum of interaction strength.

To assess whether any frequency other than 10 Hz showed a significant effect, we performed a sign-flip permutation test (1000 permutations). For each permutation, we randomly flipped the sign of each subject's spectrum, averaged the spectra across subjects, and recorded the maximum value across all frequencies except 10 Hz. These 1000 maximum values formed the null distribution, controlling for multiple comparisons across frequency. For each frequency, we then compared the observed statistic against this null distribution to derive a p -value. This test assessed whether the empirical spectrum exceeded zero beyond chance level, indicating frequency-specific interaction effects.

2.13. Heartbeat

To compare the heartbeat rate across conditions, we identified R -peaks of ECG signals and calculated inter- R -peak intervals in seconds. We assigned each interval-value to all time points between two corresponding successive R -peaks. This provided us with a continuous inter-heartbeat interval signal. Then, for each condition and each subject, we took the average across the first second (i.e., during stimulation) of all trials. For each subject, we z -scored the resulting 7 values. To normalize the data at the population level, we further divided these z -scores by their standard deviation across conditions and subjects and transformed them using a sigmoid function ($\frac{1-e^{-1.5x}}{1+e^{-1.5x}}$). A Kolmogorov–Smirnov test did not reveal any significant difference between the distribution of the transformed data and a normal distribution ($p = 0.34$).

Finally, we employed a repeated measure ANOVA to compare the transformed inter-heartbeat intervals of different conditions. Specifically, we applied a 2-way repeated measure ANOVA with factors tACS phase (0 or π), visual flicker (present or absent), and their interaction across all conditions with tACS ($VT_0, VT_{\pi}, VT_{\pi/2}, VT_{3\pi/2}, T_0$, and T_{π}).

2.14. Analysis software

All data analyses were performed in Matlab (MathWorks) using custom scripts and the open source toolbox Fieldtrip [42].

2.15. Data and materials availability

The data that support the findings of this study are available from the corresponding authors. Matlab code for constructing the composite signals, normalization, and cluster-based permutation test is available at <https://osf.io/akxhp/>.

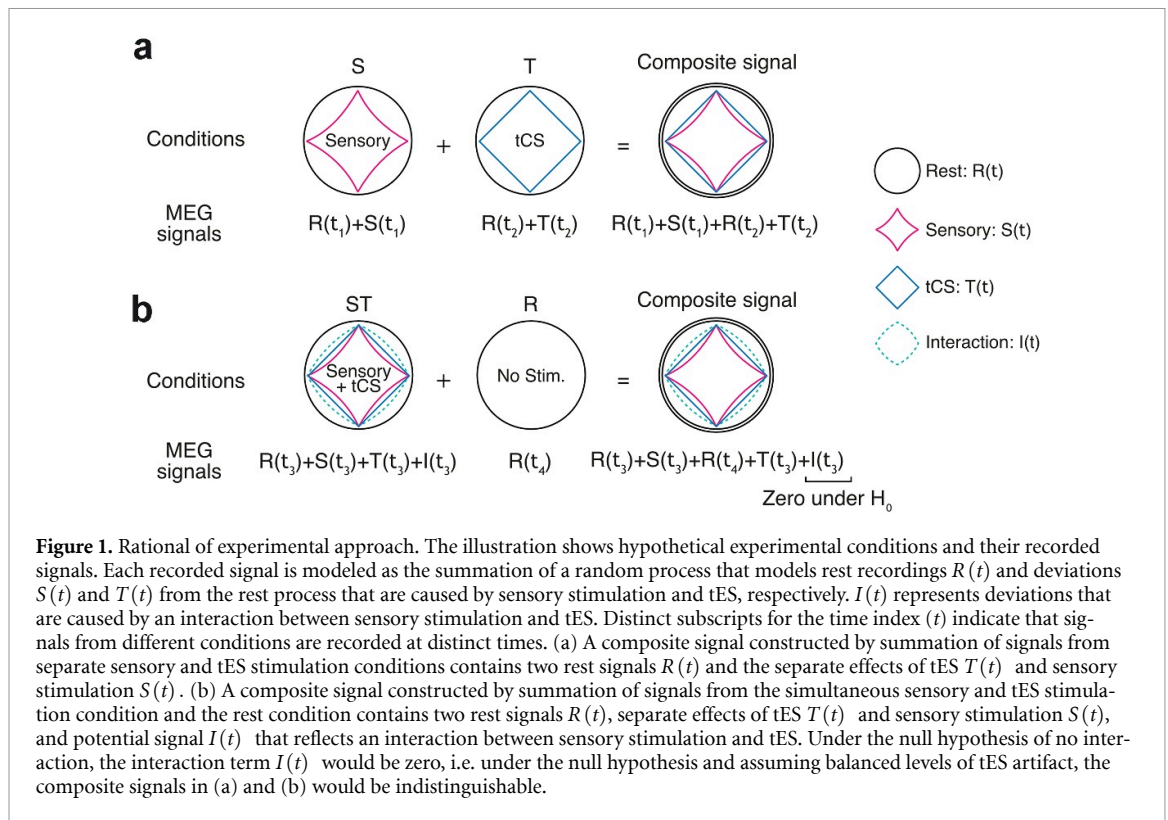
3. Results

3.1. Testing linear superposition versus interaction

To test whether tES simply superimposes on intrinsic brain activity or interacts with it, it is essential to control intrinsic activity. A practical way to achieve this is to use a sensory stimulation that elicits a reliable and well-controlled brain rhythm, providing a reference state against which the effects of tES can be compared.

At first sight, one might consider a straightforward test: add the signals recorded during sensory stimulation alone and during tES alone, and compare this sum to the signal recorded during simultaneous sensory stimulation and tES (i.e. as labeled in figure 1, compare the sum of the signals in conditions S and T with the signal in condition ST). If the two matched, this would suggest no interaction, whereas any difference would suggest a potential interaction between tES and sensory stimulation.

However, this logic is flawed. The sum of sensory stimulation alone and tES alone contains not only the



separate effects of sensory and tES stimulation, but also two copies of ongoing brain activity that is independent of stimulation (represented by the double circle for the composite signal in figure 1(a), with one copy contributed by each condition). By contrast, the simultaneous sensory stimulation and tES condition contains only one copy of ongoing brain activity. In the following we will refer to this stimulation-independent ongoing brain activity as resting activity.

To make the comparison valid, we must equalize the amount of resting activity in both cases. This is achieved by adding signals from a resting condition to the simultaneous sensory stimulation and tES signal (figure 1(b)). The result is two composite signals that are matched in resting activity, in the independent effects of sensory stimulation and tES, and potentially in their artifact content: one representing the linear superposition of sensory stimulation and tES applied separately (figure 1(a)), and one representing sensory stimulation and tES applied simultaneously (figure 1(b)).

Assuming similar artifact levels, the absence of interaction yields indistinguishable composite signals, whereas any difference between them indicates an interaction between tES and intrinsic brain activity driven by sensory stimulation. Importantly, tES artifacts are known to interact with physiological signals such as heartbeats [19–21]. Thus, physiological signals should be compared between conditions to test if artifact levels are indeed similar between conditions.

In the following, we applied this approach in a proof-of-principle MEG experiment with 10 Hz visual flicker and 10 Hz tACS at different phase relations.

3.2. Experiment and preprocessing

Sixteen subjects participated in the experiment, in which we recorded MEG signals during seven different stimulation conditions (figure 2(a)). The experiment consisted of two elements: 1 s 10 Hz visual flicker and a 1.2 s 10 Hz tACS targeting the occipital cortex (figure 2(b)). We used the 10 Hz flicker to induce steady-state brain responses with replicable phases across trials. In the context of our proposed approach, this provides defined states of intrinsic brain activity. To investigate the phase-specific interaction of tACS with intrinsic brain activity, we employed simultaneous visual flicker and tACS at four different phase differences: 0° , 90° , 180° , or 270° (conditions: VT_0 , $VT_{\pi/2}$, VT_π , $VT_{3\pi/2}$, respectively). Furthermore, there were three control conditions, during which we applied either the 10 Hz visual flicker stimulus alone (V) or 10 Hz tACS alone with an initial phase of either 0° (T_0) or 180° (T_π). For each subject, the tACS stimulation intensity was adjusted below phosphene threshold, i.e. tACS did not induce any visual percept on its own. We ran the experiment in 1.2 s trials and randomly assigned each trial to one of the seven stimulation conditions.

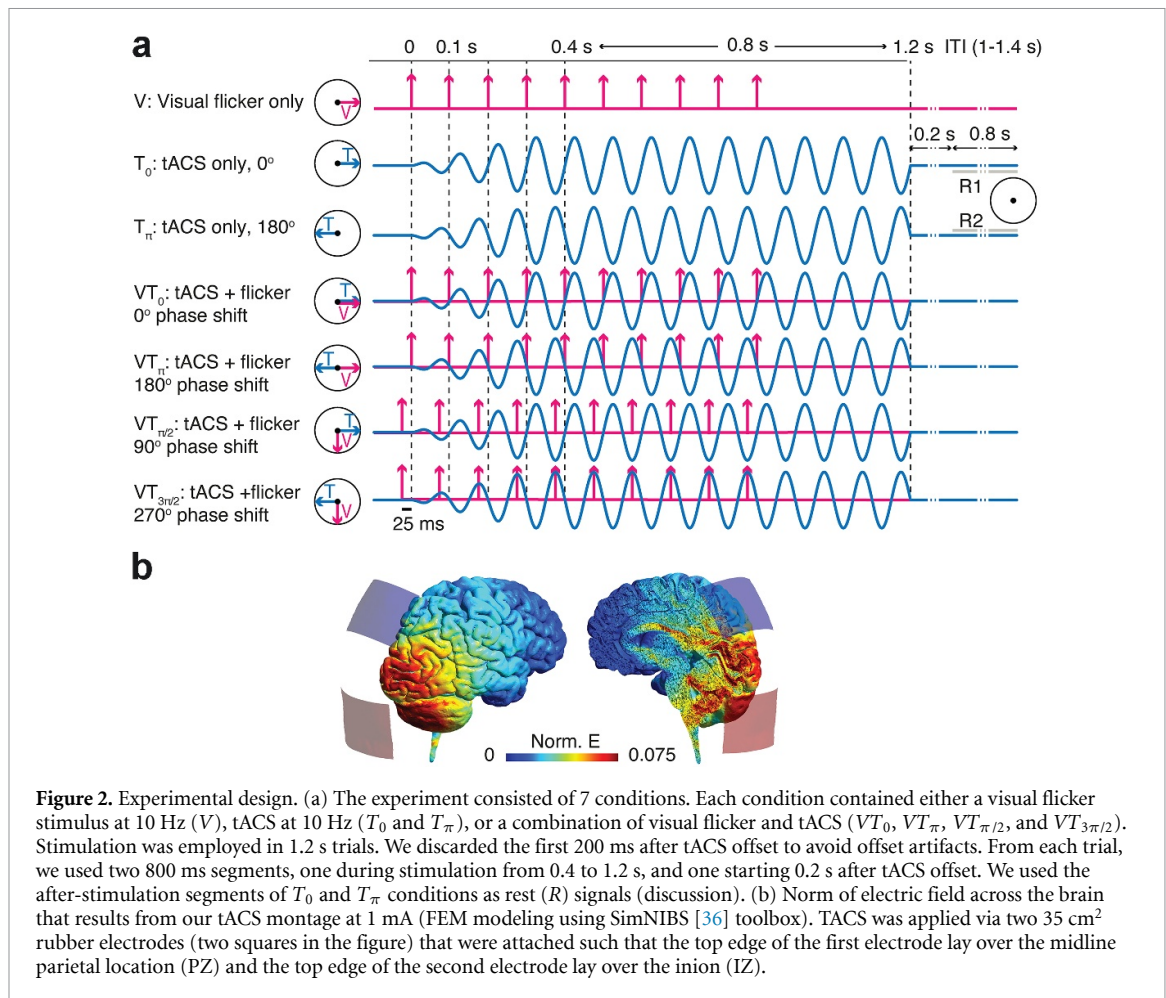


Figure 2. Experimental design. (a) The experiment consisted of 7 conditions. Each condition contained either a visual flicker stimulus at 10 Hz (V), tACS at 10 Hz (T_0 and T_π), or a combination of visual flicker and tACS (VT_0 , VT_π , $VT_{\pi/2}$, and $VT_{3\pi/2}$). Stimulation was employed in 1.2 s trials. We discarded the first 200 ms after tACS offset to avoid offset artifacts. From each trial, we used two 800 ms segments, one during stimulation from 0.4 to 1.2 s, and one starting 0.2 s after tACS offset. We used the after-stimulation segments of T_0 and T_π conditions as rest (R) signals (discussion). (b) Norm of electric field across the brain that results from our tACS montage at 1 mA (FEM modeling using SimNIBS [36] toolbox). TACS was applied via two 35 cm² rubber electrodes (two squares in the figure) that were attached such that the top edge of the first electrode lay over the midline parietal location (PZ) and the top edge of the second electrode lay over the inion (IZ).

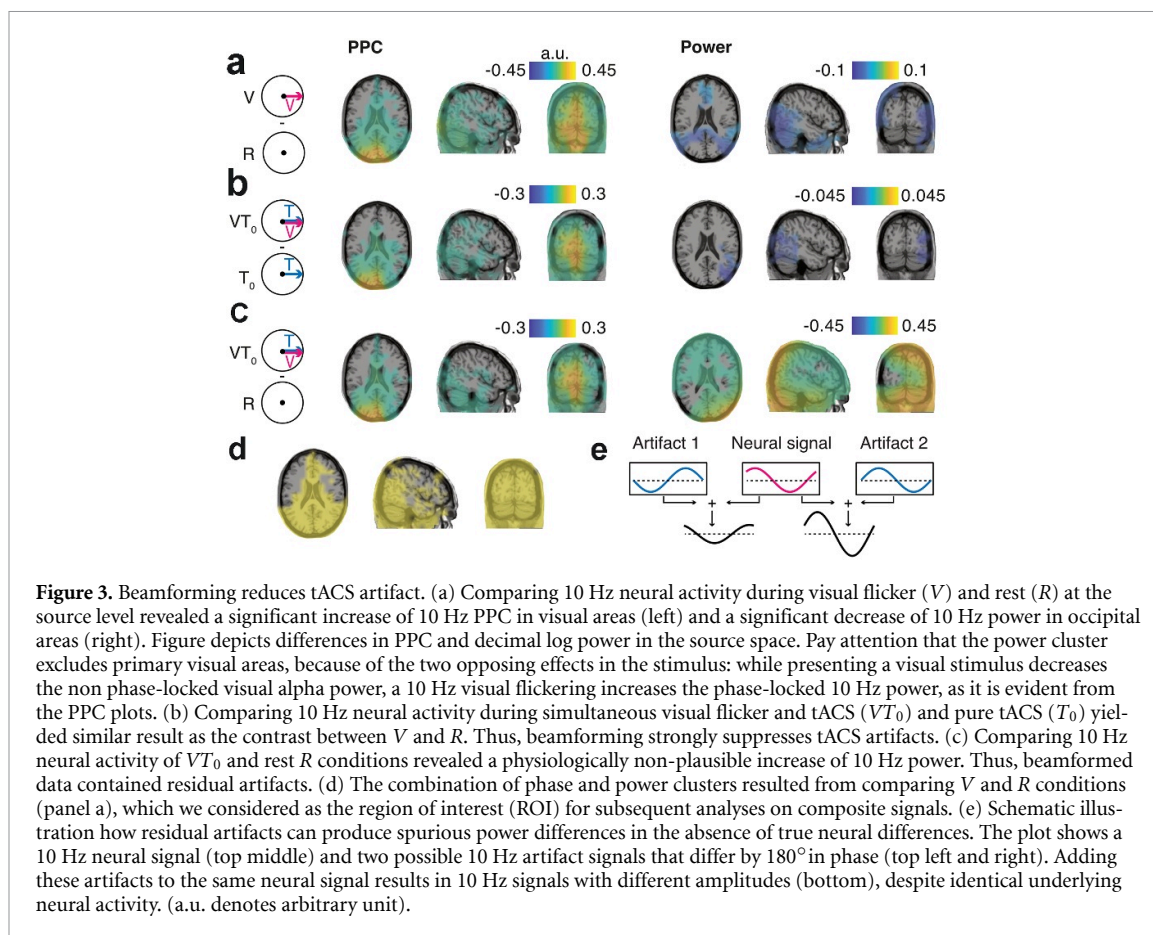
We applied beamforming (linearly constrained minimum variance, LCMV) [37] to the MEG signals to estimate neural activity at the source level. In short, beamforming is a linear transformation that estimates the source level activity, i.e. the neural activity at different brain locations from sensor level recordings.

As a first sanity check, we compared source level activity during visual flicker (V) and during rest (R) using cluster-based permutation statistics (see methods). We computed the PPC [39] to quantify the phase alignment of neural activity across trials. As expected, 10 Hz visual flicker induced a significant increase of 10 Hz PPC in visual cortex, which reflects the steady-state response of visual cortex to the flicker stimulus (figure 3(a), left). In contrast, 10 Hz power was significantly decreased during visual stimulation as compared to rest (figure 3(a), right). Compared to the increase in phase-locking, the power decrease was less pronounced and excluded the primary visual area. This reflects the opposing effects that the visual stimulus had on phase-locked and non phase-locked components of alpha-band activity [43]: while presenting a visual stimulus leads to a general decrease in non phase-locked alpha-band activity, known as alpha suppression

[44, 45], the evoked steady-state response at the flickering frequency (10 Hz) leads to an increase in the phase-locked activity at 10 Hz. In sum, visual flicker induced the expected phase-alignment of intrinsic neural activity at the stimulation frequency.

3.3. Residual artifacts at the source level

Beamforming is known to suppress tACS artifacts [19]. To assess this suppression, we again compared source-level activity with and without visual flicker, but now during tACS stimulation. In other words, we compared trials with simultaneous tACS and visual flicker against trials with pure tACS at the same initial phase (VT_0 vs T_0) (figure 3(b)). Because tACS intensity was below phosphene threshold, we expected similar results as for the comparison between visual flicker and rest conditions (figure 3(a)). Notably, due to the strong tACS artifacts, such a comparison does not lead to meaningful results at the sensor level (data not shown). However, at the source level we indeed observed effects in line with our prediction. There was a significant increase of occipital 10 Hz phase-locking and a significant decrease of 10 Hz power during simultaneous visual flicker and tACS conditions as compared to matched tACS alone conditions (figure 3(b)).



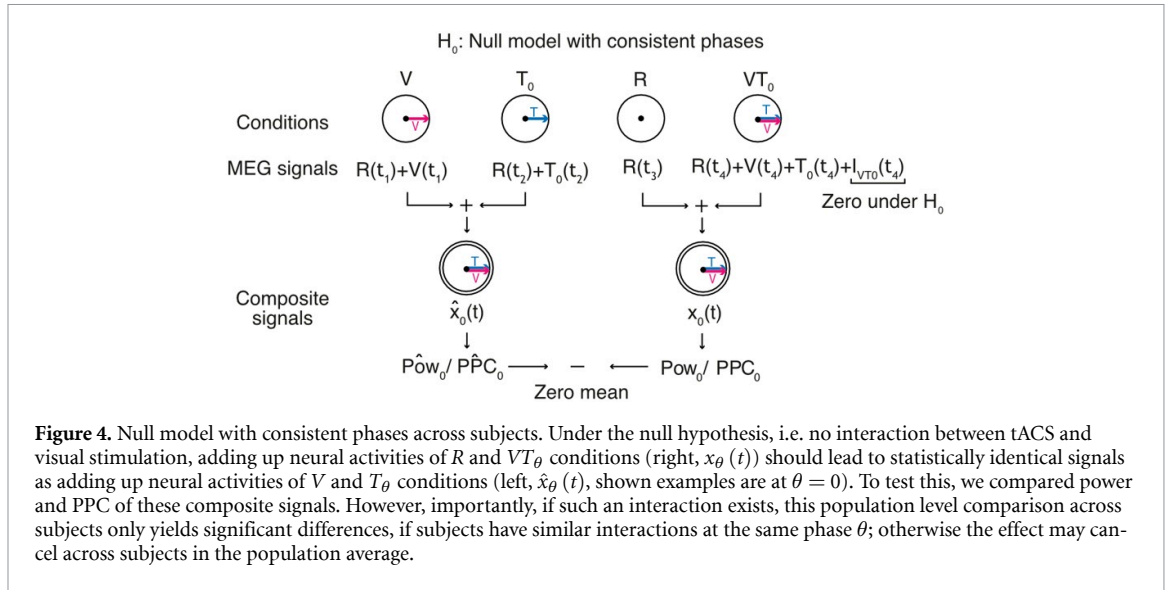
Previous studies have shown that, although beamforming suppresses tACS artifacts, it does not completely remove them [19, 20]. We confirmed this by directly comparing the source-level activity between the combined flicker and tACS condition (VT_0) and rest (R). Source-level activity during combined stimulation showed up to 260% higher 10 Hz power as compared to rest signals (figure 3(c)). For comparison, the 10 Hz suppression that we observed when comparing flicker only (V) and rest (R) conditions was less than 17% (figure 3(a)). Thus, the effect of tACS was more than 10-fold stronger than the effect of visual stimulation. Thus, while the power increase with tACS may in principle reflect effects on neural activity, the relative strength of this effect suggests that it mostly reflected residual tACS artifacts.

Such residual artifacts severely impede the study of tACS effects on neural activity during stimulation. For example, one might consider studying the interaction of 10 Hz tACS and visual flicker by comparing 10 Hz power between conditions with different relative phases, e.g. by comparing conditions VT_0 and VT_π . However, because both flicker and tACS are applied at 10 Hz in a phase-locked manner, any power difference between these two conditions could merely be due to the phase relationship of their residual artifacts. For example, as tACS in VT_0 and VT_π conditions has 180° phase difference

(figure 2), their residual artifacts might also have a phase difference of 180° . A linear summation of a flicker-evoked 10 Hz steady-state response and these residual artifacts leads to 10 Hz signals with different amplitudes (figure 3(e)). Therefore, even under the null-hypothesis of no interaction between neural effects of tACS and visual flicker, there would be a power difference between conditions with different relative stimulation phases. Therefore, to investigate neural effects during tACS, one needs to account for the strength and phase of residual artifacts. Next, we implement our proposed approach to isolate the desired neural effect.

3.4. Constructing composite signals

To test for an interaction between intrinsic neural activity driven by visual flicker and tACS, we construct composite signals from simultaneous or separate stimulation conditions. Importantly, to match tACS artifacts, the two contrasted composite signals should be constructed using pairs of VT_θ and T_θ conditions that have the exact same tACS parameters (e.g. using VT_0 and T_0 ; figure 2(a)). We took additional measures to ensure that tACS artifacts did not differ between tACS conditions. First, as tACS artifacts may change during the duration of the experiment, we recorded trials of different stimulation conditions in a randomized interleaved order (materials and methods). Second, as tACS artifacts



are known to be modulated by heart beats [19–21], we tested for heart rate differences between tACS conditions, and found no significant differences (all p -values > 0.11 ; repeated measure AVOVA with factors tACS phase (0 or π) and visual flicker (present or absent) on inter-heartbeat intervals, during tACS, and across all conditions that contain tACS). Third, to avoid any potential confound of source-reconstruction filters, we employed the same beamforming filter for all conditions. In sum, based on these measures, we assumed that, on average, MEG signals of tACS conditions with the same tACS parameters contained similar tACS artifacts.

To construct composite signals that only differ in whether they contain the potential interaction between tACS and in-phase visual flicker (VT_0), we followed the above-described logic depicted in figure 1. Replacing condition S of the general case (figure 1) with the visual flicker V (figure 4), yields the following composite signals:

$$\hat{x}_0(t) = Y_{T_0} + Y_V = R(t_1) + R(t_2) + T_0(t_2) + V(t_1) \quad (21)$$

$$x_0(t) = Y_R + Y_{VT_0} = R(t_3) + R(t_4) + T_0(t_4) + V(t_4) + I_{VT_0}(t_4) \quad (22)$$

where Y_C is the source level activity for condition C , $V(t)$ and $T_0(t)$ are the changes in the resting random process caused by the visual stimulus and 0° tACS, respectively, and $I_{VT_0}(t)$ represents the interaction term. The first composite signal (20) is the summed signals from tACS alone and visual stimulation ($\hat{x}_0(t)$, figure 4 left) and the other composite signal (21) is the summed signals from rest and combined stimulation ($x_0(t)$, figure 4 right). We constructed such composite signals for all four phase-differences ($x_\theta(t)$ and $\hat{x}_\theta(t)$, materials and methods).

Under the null hypothesis, the interaction term would be zero and therefore there should be no significant differences between the statistics of $x_\theta(t)$ and $\hat{x}_\theta(t)$. In other words, any differences between the statistics of these composite signals would indicate an interaction between tACS and intrinsic neural activity driven by visual flicker.

We applied the same cluster permutation statistic that we used for the direct contrast between conditions (figure 3) to compare the composite signals. Across subjects, we did not find any significant effect on power or phase-locking for either of the four relative phases between tACS and visual flicker across the brain ($p > 0.096$ and $p > 0.2$, corrected, for all power and phase comparisons, respectively). In other words, for each relative phase, the power or PPC was not affected by whether tACS was applied simultaneous to the visual stimulation ($x_\theta(t)$) or separately ($\hat{x}_\theta(t)$).

These results could either indicate a lack of interaction between intrinsic brain activity and tACS or may merely indicate a lack of consistency across subjects. Specifically, the phase-difference, at which visual flicker and tACS interact, may vary across subjects. In this case, the effects may average out across subjects and the preformed analysis may not reveal an interaction. Thus, we next combined the composite signals into new signals that do not rely on phase consistency across subjects (figure 5).

We assumed that, for each subject, independent of the phase of strongest interactions between tACS and visual flicker (θ), the interaction should decrease or even reverse at the opposite phase ($\theta + \pi$). Therefore, we estimated how a potential interaction was modulated by phase. To this end, we computed the absolute difference of the composite signals' power and PPC between opposite phases (figure 5(a)). If there was no interaction between neural effects of visual flicker and tACS at either θ or $\theta + \pi$, the absolute differences

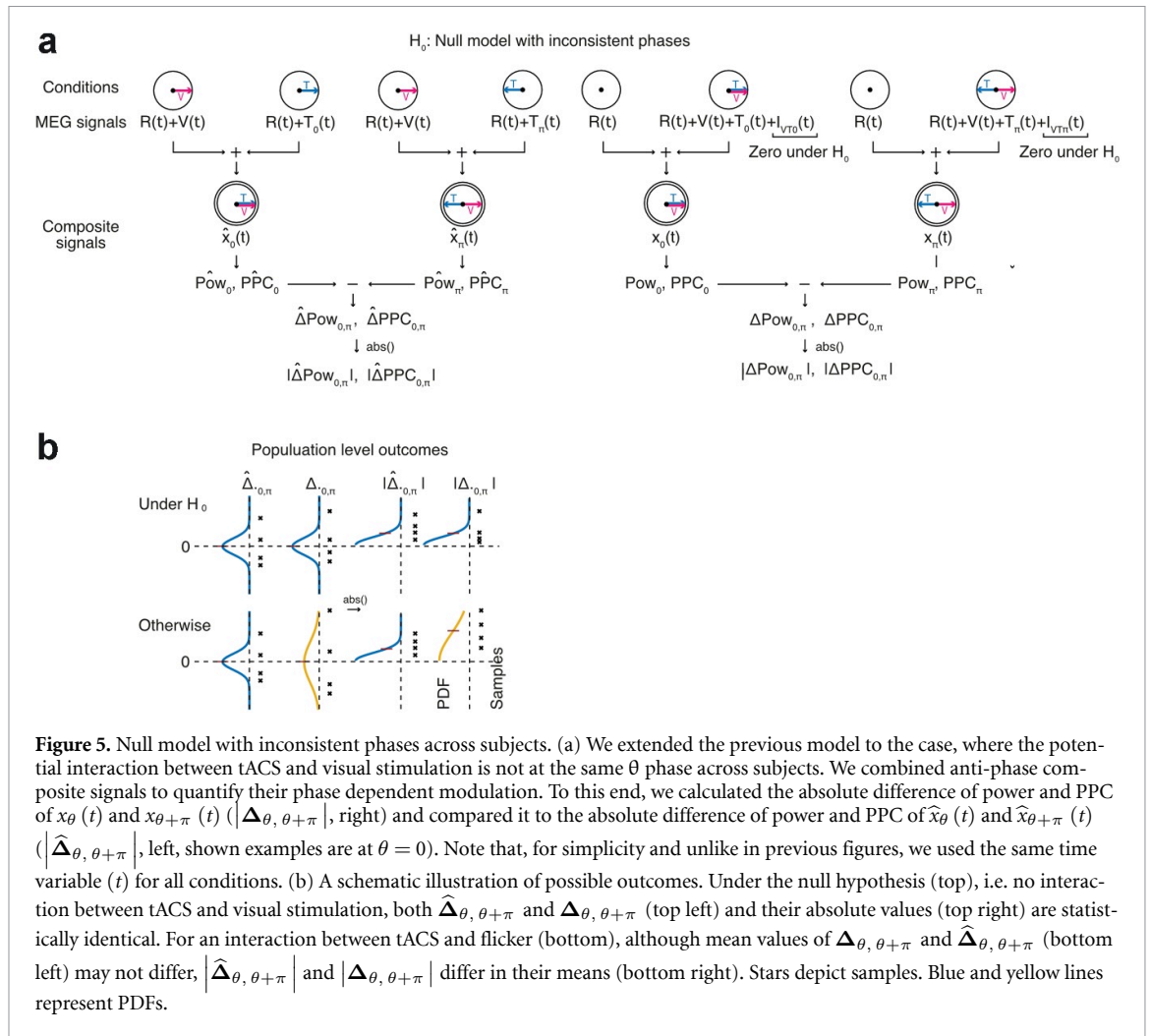


Figure 5. Null model with inconsistent phases across subjects. (a) We extended the previous model to the case, where the potential interaction between tACS and visual stimulation is not at the same θ phase across subjects. We combined anti-phase composite signals to quantify their phase dependent modulation. To this end, we calculated the absolute difference of power and PPC of $x_\theta(t)$ and $x_{\theta+\pi}(t)$ ($|\Delta_{\theta, \theta+\pi}|$, right) and compared it to the absolute difference of power and PPC of $\hat{x}_\theta(t)$ and $\hat{x}_{\theta+\pi}(t)$ ($|\hat{\Delta}_{\theta, \theta+\pi}|$, left, shown examples are at $\theta = 0$). Note that, for simplicity and unlike in previous figures, we used the same time variable (t) for all conditions. (b) A schematic illustration of possible outcomes. Under the null hypothesis (top), i.e. no interaction between tACS and visual stimulation, both $\Delta_{\theta, \theta+\pi}$ and $\hat{\Delta}_{\theta, \theta+\pi}$ (top left) and their absolute values (top right) are statistically identical. For an interaction between tACS and flicker (bottom), although mean values of $\Delta_{\theta, \theta+\pi}$ and $\hat{\Delta}_{\theta, \theta+\pi}$ (bottom left) may not differ, $|\hat{\Delta}_{\theta, \theta+\pi}|$ and $|\Delta_{\theta, \theta+\pi}|$ differ in their means (bottom right). Stars depict samples. Blue and yellow lines represent PDFs.

obtained from x and \hat{x} signals should be statistically equal (figure 5(b) top). Instead, if visual flicker and tACS interacted, absolute differences between opposite phases should be larger for the simultaneous stimulation (x) than for the separate stimulations (\hat{x}) (figure 5(b) bottom).

As a first step, we applied this analysis to simulated data without any interaction (i.e. under the null hypothesis) and confirmed that the statistic was unbiased and did not produce false positives (materials and methods). Then, we performed this analysis on our dataset, again using the same cluster permutation statistic. This revealed an occipital cluster, in which 10 Hz power indicated an interaction between simultaneous 10 Hz tACS and visual flicker for relative phases of 0 and π (figure 6(a), $p = 0.032$, corrected for multiple comparisons). Phase-locking (all $p > 0.19$, corrected) or other relative phases for power ($p = 0.11$, corrected) did not yield significant effects.

To assess whether this cluster might reflect residual tACS artifacts rather than true neural modulation, we examined its spectral profile. Specifically, we tested whether the average signal within the cluster exhibited peaks at harmonic frequencies of the tACS

frequency, which would suggest artifact contamination. However, no other frequency showed a significant effect within the cluster (figure 6(c), all $p > 0.3$; materials and methods), suggesting that the observed effect was not driven by residual artifacts. In sum, two of the anti-phase conditions involving simultaneous tACS and visual flicker (i.e. VT_0 vs VT_π) revealed power differences that could not be explained without assuming an interaction between the neural effects of tACS and visual flicker. This provides evidence for a phase-dependent interaction between tACS and intrinsic neural activity driven by visual flicker.

We further directly investigated whether the absolute preferred phase of interaction was consistent across subjects. To this end, we removed the absolute value operator, and compared power and PPC between opposite phases for the identified occipital cluster. This did not yield any significant difference for either power or PPC (all $p > 0.19$, figure 6(b), left). Moreover, in another analysis, we removed the absolute value operator and re-ran the analysis across the entire source-space. Again, we did not find any significant cluster for either power or PPC (all $p > 0.14$). Therefore, in agreement with the results of the first

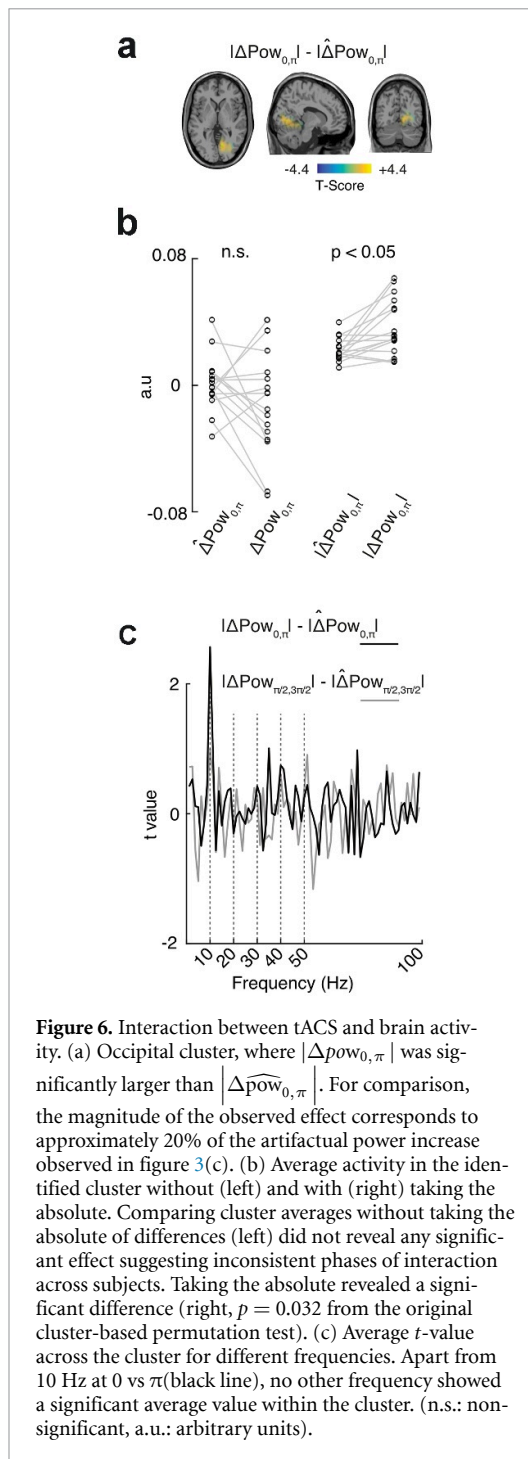


Figure 6. Interaction between tACS and brain activity. (a) Occipital cluster, where $|\Delta pow_{0,\pi}|$ was significantly larger than $|\Delta \widehat{pow}_{0,\pi}|$. For comparison, the magnitude of the observed effect corresponds to approximately 20% of the artifactual power increase observed in figure 3(c). (b) Average activity in the identified cluster averages without taking the absolute (left) and with (right) taking the absolute of differences (left) did not reveal any significant effect suggesting inconsistent phases of interaction across subjects. Taking the absolute revealed a significant difference (right, $p = 0.032$ from the original cluster-based permutation test). (c) Average t -value across the cluster for different frequencies. Apart from 10 Hz at 0 vs π (black line), no other frequency showed a significant average value within the cluster. (n.s.: non-significant, a.u.: arbitrary units).

approach (figure 4), we concluded that the phase dependency of the interaction between tACS and visual flicker was subject specific.

In principle, tACS effects may outlast the stimulation period. Thus, in a final analysis, we tested if the observed interaction effect was detectable after stimulation offset. To this end, we performed the same cluster permutation analysis on 800 ms intervals starting 200 ms after stimulation offset. The 200 ms offset ensured that intervals were free of tACS offset artifacts. Because this interval was artifact free and to increase the sensitivity of our analysis, we simply

compared VT conditions with opposite phases (i.e. VT_0 vs VT_π and $VT_{\pi/2}$ vs $VT_{3\pi/2}$). None of the tests on either power or phase yielded a spatial cluster with a significant difference (all p -values > 0.05). Therefore, we concluded that the observed interaction between tACS and intrinsic brain activity was restricted to the stimulation period.

4. Discussion

Here, we present a new approach to account for stimulation artifacts and study neural effects of tES. We propose to control intrinsic brain activity with sensory stimulation and test whether neural activity during simultaneous sensory stimulation and tES matches the linear superposition of the effects of each applied alone. Instead of attempting to obtain artifact-free signals, we construct and compare composite signals that contain similar levels of tES artifact but potentially differ in the interaction between tES and intrinsic brain activity. We applied this approach in a proof-of-principle MEG experiment with 10 Hz visual flicker and 10 Hz tACS. We employed beamforming to estimate source level activity and found a phase-dependent interaction between tACS and intrinsic neural activity driven by visual flicker.

4.1. Composite signals and residual artifacts

Our proposed approach requires that the composite signals being compared must only differ in the potential interaction between tES and the underlying brain activity and contain similar levels of tES artifacts. In other words, there should not be any systematic differences between the artifact of various conditions. Because tES artifacts cannot be recorded in isolation, we suggest an indirect strategy for addressing this prerequisite: monitoring physiological signals to compare artifact levels across conditions. TES artifacts in EEG and MEG do not only depend on tES parameters (e.g. montage, stimulation intensity, and frequency) but also on body impedance and head position (the latter is only relevant for MEG). Physiological processes such as heartbeat and respiration modulate these factors and, consequently, the characteristics of tES artifacts [19–21]. Therefore, to ensure comparable artifact levels across conditions, we recommend continuously recording physiological signals during stimulation and neural recordings. In our proof-of-principle experiment, we monitored and excluded effects on heart rate. Future studies may also monitor additional physiological variables such as body impedance, head position and respiration rate.

Because the physiological state of participants influences tES artifacts, it is important to avoid any temporal bias in the order of condition presentation. In the case of MEG, such randomization also helps to avoid systematic differences in head position across

conditions. Assuming that the MEG artifact amplitude decreases with distance as $1/r^2$ to $1/r^3$, a small displacement Δr would produce a relative change of $\Delta A/A \approx 2\Delta r/r$ to $3\Delta r/r$. Therefore, for a representative sensor–head distance of $r \approx 30$ mm, a displacement of $\Delta r \approx 2$ – 3 mm could lead to an approximately 20% artifact modulation, corresponding to the magnitude of the observed effect (figure 6(a)) relative to the artifactual power increase shown in figure 3(c). To avoid such systematic differences in our proof-of-principle study, we optimized the sequence in which the seven experimental conditions were applied. Specifically, we randomized trials in successive blocks, with each block containing one trial from each condition. This protocol ensured that slow changes in tES artifacts, such as those caused by gradual head movement or slow physiological fluctuations [19], would affect all conditions equally and minimize systematic bias due to condition order.

Finally, it is worth noting that in the present study we used post-stimulation segments as rest to construct the composite signals. In principle, these post-stimulation segments could contain residual offset artifacts or outlasting neural influences of tACS. In such a case, contrasting the constructed composite signals would be compromised, because rest signals would be unevenly represented across composite signals (figures 1, 4, and 5). However, we did not observe any significant differences between post-stimulation segments of tACS alone conditions with opposite phases (see materials and methods, tACS offset artifacts), arguing against a systematic contribution of offset artifacts or phase-specific outlasting tACS influences. Nevertheless, future studies could include an independent rest condition to further minimize potential asymmetries in the construction of composite signals.

4.2. Retina and the stimulation amplitude

It is important to realize that the proposed approach for detecting online interactions between tACS and neural activity is neutral with respect to the site of interaction between stimulation and neural activity. Thus, it is important to critically consider the possible physiological origins of the observed interaction, and in particular, whether it originates at the cortical or retinal level.

In the presented study, we kept the tACS amplitude below individual phosphene thresholds to minimize retinal stimulation. This resulted in an average stimulation amplitude of 0.4 ± 0.16 mA (mean \pm std, 0.8 peak to peak), which translates to induced cortical electrical fields of about 0.16 V m⁻¹ [46]. Although this is below the intensities often used in tACS studies [46, 47], previous invasive studies have shown that even at such low stimulation intensities network level modulations are observable. For example, Reato *et al* [48] observed robust entrainment effects in brain

slices exposed to electric fields as low as 0.2 V m⁻¹, and Huang *et al* [49] reported significant effects in the ferret brain at stimulation intensities as low as about 0.11 V m⁻¹, when applied at individual alpha frequencies. Therefore, our findings are consistent with previous studies using weak tES intensities. Increasing the stimulation amplitude in future experiments may enhance the neural interaction effects, potentially leading to the identification of stronger and more widespread effects.

One further observation is consistent with a cortical-level interaction. Visual flicker exerted two opposing effects on occipital 10 Hz power: a suppression of non-phase-locked alpha activity and an increase in phase-locked activity at the flicker frequency. These opposing effects are evident in figure 3(a), where the alpha power decrease is absent in voxels showing the strongest phase locking. Notably, the interaction cluster in figure 6(a) is located in a region where these two influences appear to compete, rather than at locations exhibiting maximal phase locking or maximal power suppression. This is consistent with an interaction occurring at the level of visual cortex.

However importantly, despite the comparatively weak stimulation, the absence of phosphene perception and the nature of observed effects, a retinal origin of the observed interaction cannot be excluded based on the present data. Indeed, the employed tACS montage is not optimally focal and may also stimulate the retina [4, 50]. Future studies employing more focal stimulation montages are required to increase the ratio of cortical to retinal stimulation [36, 51–54] and to further clarify the contribution of retinal mechanisms to interactions between tACS and intrinsic brain activity.

4.3. Nonlinearities in brain function

The observed interaction between the neural effects of tACS and visual flicker imply a non-additive interaction between neural effects of tACS and visual flicker. Such nonlinearities have been reported in several previous tES studies [9, 11, 23–33]. One of the early examples of such interactions shows that the effect of transcranial direct current stimulation on motor performance depends on its timing relative to motor training [31]. Such dependencies have been also shown for tACS. For example, keeping the eyes closed during tACS decreases the aftereffects of occipital alpha tACS on alpha power [30]. In another study, Lustenberger *et al* have shown that application of tACS locked to sleep spindles enhances motor memory consolidation [27]. Such interactions may be particularly important for tACS, for which only a small fraction of the applied currents effectively reaches the brain [51]. Therefore, it is critical to establish circumstances, under which tACS currents

show their maximal effectiveness [55]. In the current study, we employed visual flicker to provide such circumstances.

The proposed approach could be readily extended to other brain areas and sensory stimulation protocols. Importantly, this extension presupposes the availability of an experimental manipulation that induces a stable and predictable underlying brain state. Thus, the applicability of the present framework is constrained in two respects. First, the framework is not suitable for isolating tACS neural effects during the resting state. Second, it must be possible to reliably induce the desired underlying brain activity via external stimulation or task-related factors. In the current paper, we emphasized sensory stimulation to induce such brain states. Whether cognitive tasks could also serve this purpose remains to be investigated in future studies.

The nervous system shows a broad spectrum of non-linear behaviors from spike generation and synaptic integration to network interaction effects. In principle, any of such non-linearities may underlie the observed interaction between tACS and intrinsic neural activity. For example, without visual stimulation, weak tACS currents may induce sub-threshold membrane potential fluctuation with only weak effects on spiking activity. Visual flicker may bring neurons closer to their firing threshold, such that simultaneous tACS currents would induce stronger effects on spiking activity than without visual stimulation. Computational modeling and further studies—in particular invasive ones—are required to clarify the mechanisms underlying the observed interaction.

It is worth noting that we did not observe any tACS effects directly after stimulation offset. This is compatible with other previous studies that report stimulation effects restricted to the stimulation period [13, 56]. For the present experiments, the lack of long-lasting effects may also be due to the relatively weak and short stimulation protocol. Indeed, a recent study that applied longer tACS and visual flicker stimuli as compared to the present experiments, found a similar interaction after tACS offset, which manifested in a lasting modulation of steady-state responses to visual flicker [57].

4.4. Future directions

The present study establishes a basis for several avenues of future research. First, as outlined above, future work should measure a broader set of physiological parameters and use more focal stimulation montages to better rule out artifact confounds and clarify retinal contributions. It will be important to replicate our proof-of-principle findings under these conditions. Second, varying stimulation parameters could help to further elucidate the origins of the observed effects. For instance, increasing stimulation amplitude may

yield more pronounced interactions, and dissociating the frequencies of tACS and sensory stimulation would provide a valuable control. For example, no interaction is expected when the tACS and visual flicker frequencies lack a harmonic relationship (e.g. tACS at 10 Hz and flicker at 25 Hz).

4.5. Conclusion

In summary, our work establishes a new strategy to study online neural effects of tACS and provides direct evidence for a state-dependent and subject-specific interaction of tACS with intrinsic brain activity.

Acknowledgment

This study was supported by the European Research Council (ERC) StG 335880 and CoG 864491 (M. S.), and the Centre for Integrative Neuroscience (DFG, EXC 307) (M. S.).

Data availability statement

The data that support the findings of this study are available upon reasonable request from the authors.

Author contributions

Conceptualization: M. S., N. N.; investigation: N. N., F. D.; formal analysis: N. N.; writing—original draft preparation: N. N.; writing—review and editing: N. N., M. S.; supervision: M. S., N. N.; resources: M. S.; funding acquisition: M. S.

Conflict of interest

All authors declare no competing interests.

ORCID iDs

Nima Noury  0000-0002-2721-3423

Fabio Damiani  0009-0003-4317-5134

Markus Siegel  0000-0001-5115-936X

References

- [1] Dmochowski J P, Datta A, Bikson M, Su Y and Parra L C 2011 Optimized multi-electrode stimulation increases focality and intensity at target *J. Neural Eng.* **8** 046011
- [2] Kanai R, Chaieb L, Antal A, Walsh V and Paulus W 2008 Frequency-dependent electrical stimulation of the visual cortex *Curr. Biol.* **18** 1839–43
- [3] Schutter D J L G and Hortensius R 2010 Retinal origin of phosphenes to transcranial alternating current stimulation *Clin. Neurophysiol.* **121** 1080–4

- [4] Schwiedrzik C M 2009 Retina or visual cortex? The site of phosphene induction by transcranial alternating current stimulation *Front. Integr. Neurosci.* **3** 970
- [5] Antal A et al 2025 Low intensity transcranial electric stimulation: safety, ethical, legal regulatory and application guidelines (2017–2025: an update)—endorsed by the European Society for Brain Stimulation (ESBS) and by the International Federation for Clinical Neurophysiology (IFCN) *Clin. Neurophysiol.* **184** 2111436
- [6] Vieira P G, Krause M R, Laamerad P and Pack C C 2025 Brain stimulation preferentially influences long-range projections *Sci. Adv.* **11** eadx2106
- [7] Wischniewski M, Alekseichuk I and Opitz A 2023 Neurocognitive, physiological, and biophysical effects of transcranial alternating current stimulation *Trends Cognit. Sci.* **27** 189–205
- [8] Herrmann C S, Rach S, Neuling T and Strüber D 2013 Transcranial alternating current stimulation: a review of the underlying mechanisms and modulation of cognitive processes *Front. Hum. Neurosci.* **7** 279
- [9] Krause M R, Vieira P G, Thivierge J P and Pack C C 2022 Brain stimulation competes with ongoing oscillations for control of spike timing in the primate brain *PLoS Biol.* **20** e3001650
- [10] Kemmerer S K, Sack A T, de Graaf T A, ten Oever S, De Weerd P and Schuhmann T 2022 Frequency-specific transcranial neuromodulation of alpha power alters visuospatial attention performance *Brain Res.* **1782** 147834
- [11] Fröhlich F and McCormick D A 2010 Endogenous electric fields may guide neocortical network activity *Neuron* **67** 129–43
- [12] Ozen S, Sirota A, Belluscio M A, Anastassiou C A, Stark E, Koch C and Buzsáki G 2010 Transcranial electric stimulation entrains cortical neuronal populations in rats *J. Neurosci. J. Soc. Neurosci.* **30** 11476–85
- [13] Johnson L, Alekseichuk I, Krieg J, Doyle A, Yu Y, Vitek J, Johnson M and Opitz A 2020 Dose-dependent effects of transcranial alternating current stimulation on spike timing in awake nonhuman primates *Sci. Adv.* **6** eaaz2747
- [14] Wischniewski M, Tran H, Zhao Z, Shirinpour S, Haigh Z J, Rottevel J, Perera N D, Alekseichuk I, Zimmermann J and Opitz A 2024 Induced neural phase precession through exogenous electric fields *Nat. Commun.* **15** 1687
- [15] Ruhnau P, Neuling T, Fuscá M, Herrmann C S, Demarchi G and Weisz N 2016 Eyes wide shut: transcranial alternating current stimulation drives alpha rhythm in a state dependent manner *Sci. Rep.* **6** 27138
- [16] Helfrich R F, Schneider T R, Rach S, Trautmann-Lengsfeld S A, Engel A K and Herrmann C S 2014 Entrainment of brain oscillations by transcranial alternating current stimulation *Curr. Biol.* **24** 333–9
- [17] Yan X, Boudrias M H and Mitsis G D 2022 Removal of transcranial alternating current stimulation EEG artifacts using blind source separation and wavelets *IEEE Trans. Biomed. Eng.* **69** 3183–92
- [18] Haslacher D, Narang A, Sokoliuk R, Cavallo A, Reber P, Nasr K, Santarnecchi E and Soekadar S R 2023 In vivo phase-dependent enhancement and suppression of human brain oscillations by transcranial alternating current stimulation (tACS) *NeuroImage* **275** 120187
- [19] Noury N and Siegel M 2018 Analyzing EEG and MEG signals recorded during tES, a reply *NeuroImage* **167** 53–61
- [20] Noury N, Hipp J F and Siegel M 2016 Physiological processes non-linearly affect electrophysiological recordings during transcranial electric stimulation *NeuroImage* **140** 99–109
- [21] Noury N and Siegel M 2017 Phase properties of transcranial electrical stimulation artifacts in electrophysiological recordings *NeuroImage* **158** 406–16
- [22] Kasten F H, Negahbani E, Fröhlich F and Herrmann C S 2018 Non-linear transfer characteristics of stimulation and recording hardware account for spurious low-frequency artifacts during amplitude modulated transcranial alternating current stimulation (AM-tACS) *NeuroImage* **179** 134–43
- [23] Schmidt S L, Iyengar A K, Foulser A A, Boyle M R and Fröhlich F 2014 Endogenous cortical oscillations constrain neuromodulation by weak electric fields *Brain Stimul.* **7** 878–89
- [24] Romei V, Thut G and Silvanto J 2016 Information-based approaches of noninvasive transcranial brain stimulation *Trends Neurosci.* **39** 782–95
- [25] Guerra A, Pogosyan A, Nowak M, Tan H, Ferreri F, Lazzaro V D and Brown P 2016 Phase dependency of the human primary motor cortex and cholinergic inhibition cancelation during beta tACS *Cereb. Cortex* **26** 3977–90
- [26] Alekseichuk I, Turi Z, Amador de Lara G, Antal A and Paulus W 2016 Spatial working memory in humans depends on theta and high gamma synchronization in the prefrontal cortex *Curr. Biol.* **26** 1513–21
- [27] Lustenberger C, Boyle M R, Alagapan S, Mellin J M, Vaughn B V and Fröhlich F 2016 Feedback-controlled transcranial alternating current stimulation reveals a functional role of sleep spindles in motor memory consolidation *Curr. Biol.* **26** 2127–36
- [28] Berényi A, Belluscio M, Mao D and Buzsáki G 2012 Closed-loop control of epilepsy by transcranial electrical stimulation *Science* **337** 735–7
- [29] Brittain J S, Probert-Smith P, Aziz T Z and Brown P 2013 Tremor suppression by rhythmic transcranial current stimulation *Curr. Biol.* **23** 436–40
- [30] Neuling T, Rach S and Herrmann C S 2013 Orchestrating neuronal networks: sustained after-effects of transcranial alternating current stimulation depend upon brain states *Front. Hum. Neurosci.* **7** 161
- [31] Reis J and Fritsch B 2011 Modulation of motor performance and motor learning by transcranial direct current stimulation *Curr. Opin. Neurol.* **24** 590–6
- [32] Agboada D, Zhao Z and Wischniewski M 2025 Neuroplastic effects of transcranial alternating current stimulation (tACS): from mechanisms to clinical trials *Front. Hum. Neurosci.* **19** 1548478
- [33] Wansbrough K, Marinovic W, Fujiyama H and Vallence A M 2025 Beta tACS of varying intensities differentially affect resting-state and movement-related sensorimotor power *Front. Neurosci.* **19** 1524653
- [34] Kasten F H, Negahbani E, Fröhlich F and Herrmann C S 2018 Non-linear transfer characteristics of stimulation and recording hardware account for spurious low-frequency artifacts during amplitude modulated transcranial alternating current stimulation (AM-tACS) *bioRxiv Preprint* (<http://dx.doi.org/10.1016/j.neuroimage.2018.05.068>) (posted online 06 February 2018)
- [35] Brainard D H 1997 The psychophysics toolbox *Spat. Vis.* **10** 433–6
- [36] Windhoff M, Opitz A and Thielscher A 2013 Electric field calculations in brain stimulation based on finite elements: an optimized processing pipeline for the generation and usage of accurate individual head models *Hum. Brain Mapp.* **34** 923–35
- [37] Van Veen B D, van Drongelen W, Yuchtman M and Suzuki A 1997 Localization of brain electrical activity via linearly constrained minimum variance spatial filtering *IEEE Trans. Biomed. Eng.* **44** 867–80
- [38] Nolte G 2003 The magnetic lead field theorem in the quasi-static approximation and its use for magnetoencephalography forward calculation in realistic volume conductors *Phys. Med. Biol.* **48** 3637
- [39] Vinck M, van Wingerden M, Womelsdorf T, Fries P and Pennartz C M A 2010 The pairwise phase consistency: a bias-free measure of rhythmic neuronal synchronization *NeuroImage* **51** 112–22
- [40] Maris E and Oostenveld R 2007 Nonparametric statistical testing of EEG- and MEG-data *J. Neurosci. Methods* **164** 177–90

- [41] Nichols T E and Holmes A P 2002 Nonparametric permutation tests for functional neuroimaging: a primer with examples *Hum. Brain Mapp.* **15** 1–25
- [42] Oostenveld R, Fries P, Maris E and Schoffelen J M 2011 FieldTrip: open source software for advanced analysis of MEG, EEG, and invasive electrophysiological data *Comput. Intell. Neurosci.* **2011** 156869
- [43] Donner T H and Siegel M 2011 A framework for local cortical oscillation patterns *Trends Cognit. Sci.* **15** 191–9
- [44] Woodman G F, Wang S, Sutterer D W, Reinhart R M G and Fukuda K 2022 Alpha suppression indexes a spotlight of visual-spatial attention that can shine on both perceptual and memory representations *Psychon. Bull. Rev.* **29** 681–98
- [45] Klimesch W, Sauseng P and Hanslmayr S 2007 EEG alpha oscillations: the inhibition–timing hypothesis *Brain Res. Rev.* **53** 63–88
- [46] Huang Y, Liu A A, Lafon B, Friedman D, Dayan M, Wang X, Bikson M, Doyle W K, Devinsky O and Parra L C 2017 Measurements and models of electric fields in the in vivo human brain during transcranial electric stimulation. Ivry R, editor *eLife* **6** e18834
- [47] Opitz A et al 2016 Spatiotemporal structure of intracranial electric fields induced by transcranial electric stimulation in humans and nonhuman primates *Sci. Rep.* **6** 31236
- [48] Reato D, Rahman A, Bikson M and Parra L C 2010 Low-intensity electrical stimulation affects network dynamics by modulating population rate and spike timing *J. Neurosci.* **30** 15067–79
- [49] Huang W A et al 2021 Transcranial alternating current stimulation entrains alpha oscillations by preferential phase synchronization of fast-spiking cortical neurons to stimulation waveform *Nat. Commun.* **12** 3151
- [50] Paulus W 2010 On the difficulties of separating retinal from cortical origins of phosphenes when using transcranial alternating current stimulation (tACS) *Clin. Neurophysiol. J. Int. Fed. Clin. Neurophysiol.* **121** 987–91
- [51] Bland N S and Sale M V 2019 Current challenges: the ups and downs of tACS *Exp. Brain Res.* **237** 3071–88
- [52] Bortoletto M, Rodella C, Salvador R, Miranda P C and Miniussi C 2016 Reduced current spread by concentric electrodes in transcranial electrical stimulation (tES) *Brain Stimul.* **9** 525–8
- [53] Opitz A, Paulus W, Will S, Antunes A and Thielscher A 2015 Determinants of the electric field during transcranial direct current stimulation *NeuroImage* **109** 140–50
- [54] Alekseichuk I, Falchier A Y, Linn G, Xu T, Milham M P, Schroeder C E and Opitz A 2019 Electric field dynamics in the brain during multi-electrode transcranial electric stimulation *Nat. Commun.* **10** 2573
- [55] Bergmann T O, Karabanov A, Hartwigsen G, Thielscher A and Siebner H R 2016 Combining non-invasive transcranial brain stimulation with neuroimaging and electrophysiology: current approaches and future perspectives *NeuroImage* **140** 4–19
- [56] Negahbani E, Kasten F H, Herrmann C S and Fröhlich F 2018 Targeting alpha-band oscillations in a cortical model with amplitude-modulated high-frequency transcranial electric stimulation *NeuroImage* **173** 3–12
- [57] Fiene M, Schwab B C, Misselhorn J, Herrmann C S, Schneider T R and Engel A K 2020 Phase-specific manipulation of rhythmic brain activity by transcranial alternating current stimulation *Brain Stimul.* **13** 1254–62